ACS APPLIED MATERIALS & INTERFACES

Research Article

Cite This: ACS Appl. Mater. Interfaces 2018, 10, 6895−6903

www.acsami.org

Bacterial Analysis Using an Electrochemical DNA Biosensor with Poly-Adenine-Mediated DNA Self-Assembly

Lanying Li,[†] Lele Wang,[†] Qin Xu,[†] Li Xu,[†] Wen Liang,[†] Yan Li,[†] Min Ding,[†] Ali Aldalbahi,[∥] Zhilei Ge,[⊥] Lihua Wang,[⊥] Juan Yan,[§] Na Lu,[‡] Jiang Li,*[,⊥] Yanli Wen,*[,†] and Gang Liu*[,†]

[†]Laboratory of Biometrology, Division of Chemistry and Ionizing Radiation Measurement Technology, Shanghai Institute of Measurement and Testing Technology, Shanghai 201203, China

[‡]School of Materials Engineering, Shanghai University of Engineering Science, Shanghai 201620, China

[§]College of Food Science & Technology Shanghai Ocean University, Shanghai 201306, China

[∥]Chemistry Department, King Saud University, Riyadh 11451, Saudi Arabia

[⊥]Division of Physical Biology & Bioimaging Center, Shanghai Institute of Applied Physics, Chinese Academy of Science, Shanghai 201800, China

Supporting Information

ABSTRACT: The spatial arrangement of DNA probes on the electrode surface is of critical significance for the performance of electrochemical biosensors. However, rational control of the probe surface remains challenging. In this work, we develop a capture probe carrying a poly-adenine anchoring block to construct a programmable self-assembled monolayer for a "sandwich-type" electrochemical biosensor. We show that with a co-assembling strategy using a polyA capture probe and 6-mercapto-1-hexanol, the density of the probes on the gold electrode can be simply adjusted by the length of polyA. The electron-transfer effect and thus the hybridization efficiency can as well be optimized by tuning the polyA length. As a result, we obtained an excellent biosensor performance with a limit of detection as low as 5 fM for a synthetic DNA target. We demonstrate the practicability of this system by analyzing a PCR product from *Escherichia coli* genomic DNA (0.2 pg/μL). On the basis of the ideal electrochemical interface, our polyA-based biosensor exhibited excellent reusability and stability, which is important for potential applications in the onsite analysis for a wide range of targets.

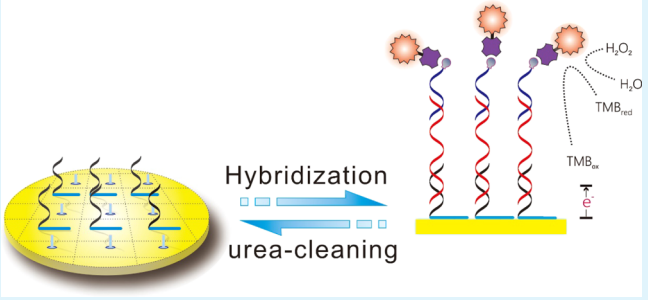

KEYWORDS: *self-assembly monolayer, poly-adenine DNA probe, electrochemical biosensor, modification-free, E. coli genome*

1. INTRODUCTION

Electrochemical nucleic acid biosensors (E-biosensor)[1−5] have attracted growing research interest as promising tools for quantitative analysis in many important areas including clinical diagnosis,[6−10] microbiological detection,[11] antibioterrorism, and environmental monitoring.[12,13] They show unique advantages such as high sensitivity, high specificity, low cost, and good portability.[14−25] For the construction of a typical electrochemical DNA biosensor,[26,27] a recognition DNA probe is immobilized onto the electrode to capture the target DNA molecules through specific hybridization, and subsequently, the biosensor will transduce the presence of the target DNA to an electrochemical signal. It is well-recognized that the performance of the sensors is highly dependent on the spatial arrangements of the self-assembled monolayer (SAM) of DNA probes on the electrode surface. In recent decades, many biosensing strategies have been focusing on building well-organized DNA SAMs,[28] including antibiofouling SAM,[29] biotin−avidin SAM,[30] and SAM on the nanoscale electrode.[31] Especially, the thiolate DNA (SH-DNA) SAM on the gold electrode has been intensively studied.[32−34] For example, Fan's group[35] demonstrated that the hybridization efficiency was highly dependent on the well-ordered upright conformation SH-DNA probes and the electron-transfer rate was highly related to the density of the DNA monolayer.[33] Nevertheless, critical obstacles still remain for rational control of the SAM organization, which restrict further improvements of the performance of DNA biosensors.

Recently, consecutive adenines (polyA) have been exploited to assemble oligonucleotides on the gold surface with a high affinity comparable to Au−S chemistry.[36−41] Pei et al. reported a polyA-mediated strategy for DNA assembly on gold nanoparticles (AuNPs) with precise amount regulation and well-organized upright conformation.[42] Later, near-unity yields of nanoparticles with fixed valences or even monovalence were obtained by tuning the length of polyA,[11] indicating the strong

Received: November 24, 2017
Accepted: January 31, 2018
Published: January 31, 2018

DOI: 10.1021/acsami.7b17327
ACS Appl. Mater. Interfaces 2018, 10, 6895−6903

Table 1. Sequences of Oligonucleotides in this Work

probe name	sequence (5′−3′)
polyA5 capture probe	A_5CCCACCAACGCTG
polyA10 capture probe	A_{10}CCCACCAACGCTG
polyA20 capture probe	A_{20}CCCACCAACGCTG
polyA30 capture probe	A_{30}CCCACCAACGCTG
polyA40 capture probe	A_{40}CCCACCAACGCTG
A5	AAAAA
reporter probe	ATCAATTCCACAGTTTTCGC-biotin
target	GCGAAAACTGTGGAATTGATCAGCGTTGGTGGGAA
PCR primer1	GCGAAAACTGTGGAATTGAT
PCR primer2	TGATGCTCCATCACTTCCTG
PCR product (250 bp)	GCGAAAACTG TGGAATTGAT CAGCGTTGGT GGGAAAGCGC GTTACAAGAA AGCCGGGCAA TTGCTGTGCC AGGCAGTTTT AACGATCAGT TCGCCGATGC AGATATTCGT AATTATGCGG GCAACGTCTG GTATCAGCGC GAAGTCTTTA TACCGAAAGG TTGGGCAGGC CAGCGTATCG TGCTGCGTTT CGATGCGGTC ACTCATTACG GCAAAGTGTG GGTCAATAAT CAGGAAGTGA TGGAGCATCA

ACS Appl. Mater. Interfaces 2018, 10, 6895−6903
DOI: 10.1021/acsami.7b17327

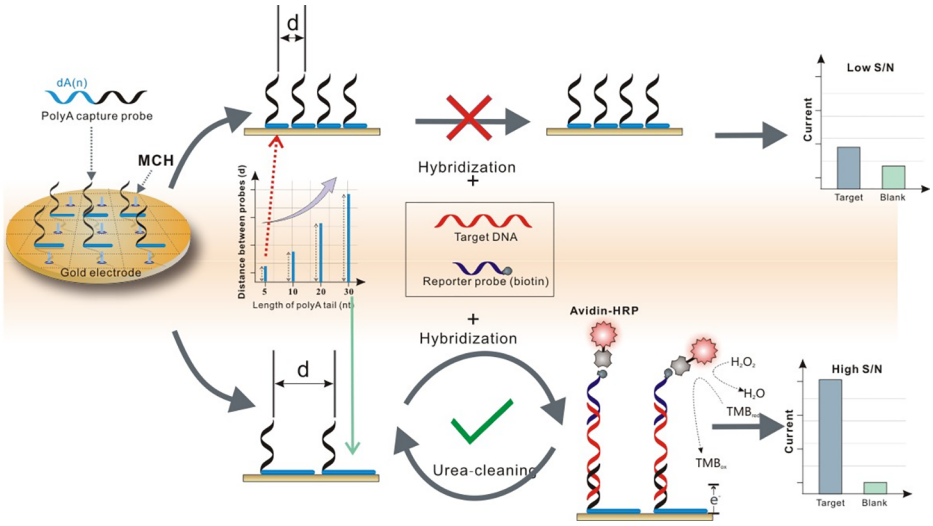

Figure 1. Schematic illustration of the polyA-based electrochemical DNA biosensor.

controllability of the DNA arrangements on the gold surface. Since then, the polyA–AuNP assembly strategy has been successfully adopted in biosensors targeting DNAs[40,43] and microRNAs[44,45] or in applications for intracellular delivery of functional nucleic acids.[46]

However, when applied to an electrochemical platform, the poor electron-transfer efficiency of the pure polyA SAM seriously hindered the signal-to-noise ratio (S/N) of the electrochemical biosensor. To develop a polyA-based electrochemical interface, in this work, we designed a novel polyA-based capture probe (polyA-P) consisting of a recognition part and a polyA anchoring block, toward a sensitive "sandwich-type" electrochemical biosensor. As a novel kind of label-free interface on the gold electrode surface, the electrochemical performance of the polyA-based SAM was systematically studied. First, different co-assembling molecules including a short oligo of five consecutive adenines (A5) and 6-mercapto-1-hexanol (MCH) were compared to achieve the optimized electron-transfer efficiency. Second, the surface density of the capture probe was precisely modulated by varying the length of the polyA block of the probe. On the basis of a series of optimization studies, we successfully developed a polyA-based electrochemical biosensor, which was applied in the analysis of a fragment of *Escherichia coli* (*E. coli*) genomic DNA, with a limit of detection (LOD) of 5 fM, and impressively, the practicability was as well demonstrated by analyzing a complex PCR product.

2. EXPERIMENTAL SECTION

2.1. Reagents. Tris(hydroxymethyl)aminomethane was purchased from Cxbio Biotechnology Ltd. Hexaammineruthenium(III) chloride ($[Ru(NH_3)_6]^{3+}$, RuHex), potassium ferricyanide ($K_3Fe(CN)_6$), ethylenediaminetetraacetic acid (EDTA), and MCH were purchased from Sigma-Aldrich (St. Louis, MO). The 3,3′,5,5′-tetramethylbenzidine (TMB) substrate was purchased from Neogen in the format of a ready-to-use reagent (TMB substrate, H_2O_2 included). The avidin-horseradish peroxidase (avidin-HRP) was purchased from eBioscience (San Diego, CA). The diluent buffer was purchased from Fitzgerald Industries International (Acton, MA). The genomic DNA extraction kit was purchased from Tiangen Biotech (Beijing) Co., Ltd. The *E. coli* strain DhSα, dNTP mixture, Ex Taq DNA polymerase, and 10× Ex Taq buffer were from Takara. All solutions were prepared in Milli-Q water (18 MΩ·cm resistivity) without further purification. All oligonucleotides were synthesized and purified by Invitrogen Inc., and the DNA sequences are shown in Table 1.

2.2. Preparation of the PolyA-P/MCH SAM on Electrode. Gold electrodes were cleaned following one of our reported work,[26] and then, the cleaned electrodes were incubated in immobilization buffer (pH 7.4, 10 mM Tris·HCl, 1 mM EDTA, 1 M NaCl) containing polyA-P of appropriate concentrations overnight under room temperature. Then, the polyA-P-modified electrodes were treated with 0.1 mM MCH to construct the interface of polyA-P/MCH SAMs. The prepared electrode was then stored in TE buffer at 4 °C overnight before being applied for DNA analysis.

2.3. Electrochemical Measurements. Step 1, the target DNA was mixed with the biotinylated reporter probe (500 nM) in 10 mM TE buffer (pH 7.4, 10 mM Tris·HCl, 1 mM EDTA) containing 1 M NaCl for 5 min under 80 °C and then cooled down to room temperature for 20 min. Step 2, the electrode with certain SAM was immersed into 150 μL solution from step 1 under 37 °C for 2 h, for the hybridization between the polyA-P and the target. Step 3, the gold electrode was rinsed with the washing buffer (pH 7.4, 10 mM Tris·HCl, 1 mM EDTA containing 0.1 M NaCl) and dried lightly with N_2 and then incubated with 3 μL of avidin-HRP (0.5 U/mL) for 15 min at room temperature. Finally, the sensors were rinsed again with a washing buffer.

A CHI 630 electrochemical workstation (CH Instruments Inc., Austin) was applied for the cyclic voltammetry (CV), amperometry (I–t), and chronocoulometry (CC) analyses, and an Autolab TYPE III (Metrohm Autolab Ltd., Switzerland) was applied for the electrochemical impedance spectroscopy (EIS) analysis. The classic three-electrode system was used throughout the experiments following a reported protocol.[57] Particularly, CC was carried out at a pulse period of 250 ms and pulse width of 700 mV, and the electrolyte buffer was thoroughly purged with N_2 before CC experiments. EIS measurement was performed in 5 mM $K_3[Fe(CN)_6]/K_4[Fe(CN)_6]$ (1:1) containing 0.1 M KCl by applying an alternating current (ac) voltage of 5 mV amplitude in a frequency range from 0.01 Hz to 100 kHz under open circuit potential.

3. RESULTS AND DISCUSSION

3.1. Design of PolyA-Based DNA Sensors. In this work, we developed a novel two-dimensional (2-D) DNA probe assembling strategy for the construction of a "sandwich-type" DNA biosensor on a gold electrode through the strong combination between polyA and gold surface, and the strategy is illustrated in Figure 1. A key element of our biosensor was polyA-P that consisted of two parts: a recognition block which could specifically capture the target DNA through hybridization

DOI: 10.1021/acsami.7b17327
ACS Appl. Mater. Interfaces 2018, 10, 6895–6903

and an anchoring block consisting of polyA which could combine to the gold electrode surface with an affinity comparable to the thiol group. Our novel label-free SAM was conveniently obtained under much lower economic cost, and of particular significance, the surface density of the probe can be easily controlled by varying the length of the polyA block. In the presence of the target DNA, the capture probe and the biotinylated reporter probe formed a sandwich-like structure on the gold electrode surface, and then, the biotin-labeled reporter probe could specifically capture an avidin-HRP. With the help of a commercially purchased TMB co-substrate (H_2O_2 contained), the HRP enzyme could produce an enzyme catalytic signal that is quantitatively related to the amount of target DNA.

3.2. EIS Characterization of the SAM. To investigate the establishing process of the polyA-based biosensor, EIS was performed after each step of the experiment in the solution of a classic electrochemical probe $[Fe(CN)_6]^{3-/4-}$. The equivalent circuit (the inset of Figure 2) was chosen to calculate the

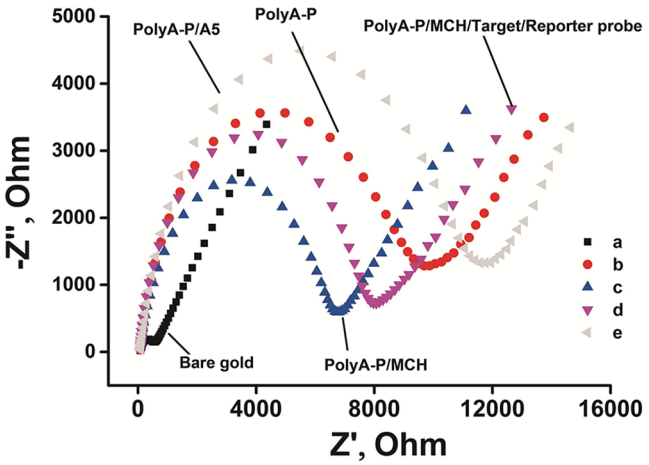

Figure 2. The Nyquist plot for electrochemical impedance measurements performed at different steps on gold electrode: (a) bare gold, (b) after polyA-P assembling (the length of polyA fragment is 30 nt in this experiment), (c) after the MCH passivation (polyA-P/MCH), (d) after the addition of target DNA and reporter probe (polyA-P/MCH/target/reporter probe), and (e) MCH was replaced with A5 in the passivation step (polyA-P/A5). All the experiments were performed in 5 mM $K_3[Fe(CN)_6]/K_4[Fe(CN)_6]$ solution containing 0.1 M KCl. The concentration of the target DNA was 1 nM.

obtained impedance data. The components in the equivalent circuit included the charge-transfer resistance (R_{et}), C_{dl} related to the interfacial double layer capacity, the diffusion impedance (Z_w), and the solution resistance (R_s). R_{et} of the electrode accounts for the diameter of the semicircle in the Nyquist plot. Figure 2 shows the results in the form of Nyquist plots. The EIS of bare gold electrode exhibited a quite low electron-transfer resistance (R_{et} = 0.5 kΩ, Figure 2a), indicating a very fast electron transfer. When polyA-P was immobilized onto the electrode surface, the EIS dramatically increased (R_{et} = 9.2 kΩ, Figure 2b) because of an increased density of negative charge and consequently increased electrostatic repulsion for $[Fe(CN)_6]^{3-/4-}$ anions. Subsequently, the resultant electrode surface was treated with MCH, leading to an obvious decrease of the electron-transfer resistance (R_{et} = 6.5 kΩ, Figure 2c), which was attributed to the competitive displacement of the unspecific adsorption of DNA molecules. Finally, the complex of target DNA and reporter probe was added to the polyA-P-covered electrode, and accordingly, we observed that the electron-transfer resistance increased (R_{et} = 8.3 kΩ, Figure 2d), indicating a fact that the hybridization brought a higher density of negative charge. Interestingly, when the polyA-P-modified gold electrode was treated with A5 instead of MCH, the electron-transfer resistance was even higher than polyA-P (R_{et} = 11.0 kΩ, Figure 2e), probably because a more compact negatively charged monolayer was formed that insulted the $Fe(CN)_6]^{3-/4-}$ anions from the electrode surface with the addition of A5.

3.3. Construction of PolyA-Based SAM. *3.3.1. Co-Assembling of MCH for Optimized Electron-Transfer Effect.* In previously reported studies, polyA-DNA has shown the capability to precisely control its density, orientation, and conformation on the surface of the nanogold particles (AuNPs), which greatly facilitates the hybridization with the target. However, when applied in the electrochemical analysis, the poor electron-transfer effect was found to be a critical disadvantage toward a highly sensitive biosensor, maybe because the compact layer of DNA molecules (~2 nm) hindered the TMB substrate from penetrating the SAM and contacting the electrode surface. Thus, in our work, two different co-assembling molecules (MCH and A5) were tested and compared using different analysis methods for a better electron-transfer effect:

3.3.2. CV Investigation of Different SAMs. When CV was performed, TMB exhibits two pairs of characteristic redox peaks on the bare gold electrode; however, when polyA-P was immobilized onto the gold electrode, the reduction peak at about 0.3 V decreased dramatically, indicating the fact that the electron transfer was impeded (Figure 3A, blue line). Then, a very similar electrochemical performance was also achieved when we immobilized A5 (3′-AAAAA-5′) together with the polyA-P on the electrode surface (polyA-P/A5) (Figure 3A, red line). In comparison, when the electrode was modified with a mixture of polyA-P and MCH, two pairs of well-defined peaks corresponding to the reduction and oxidation of TMB were observed (Figure 3A, black curve), probably because MCH competitively prevented or removed the unspecific adsorption on the surface and helped the polyA probes to keep upright on the electrode surface, and thus improved the electron-transfer efficiency on the electrode surface (Figure 3D).

3.3.3. Electron-Transfer Rate of Different SAMs. The electron-transfer rate of different SAMs in our research was then further investigated by CV in 10 mM $K_3Fe(CN)_6$ containing 0.1 M KCl. All the CV curves are shown in Figure S1. With the scan rate increased, the redox peak currents (i_p) of the gold electrodes increased accordingly, accompanied by an enlarged peak-to-peak separation (ΔE_p). With increased CV scan rate between 100 and 600 mV/s, the redox peak current increased linearly with the scan rate, indicating a typical surface-controlled electrode process. According to Laviron's equation: $k_s = mnFv/RT$,[47] where m is a parameter related to the peak-to-peak separation, F is the Faraday constant, R is the gas constant, T is the temperature, and n is the number of electrons transferred, the electron-transfer rate constant value k_s was estimated to be 0.65 s^{-1} for bare gold electrode, 0.01 s^{-1} for pure polyA-P-modified electrode, 0.07 s^{-1} for polyA-P/MCH-modified electrode, and 0.01 s^{-1} for polyA-P/A5-modified electrode, indicating the effect of MCH for an obviously optimized electron-transfer rate, which is consistent with the CV curve analysis in the last part.

DOI: 10.1021/acsami.7b17327
ACS Appl. Mater. Interfaces 2018, 10, 6895−6903

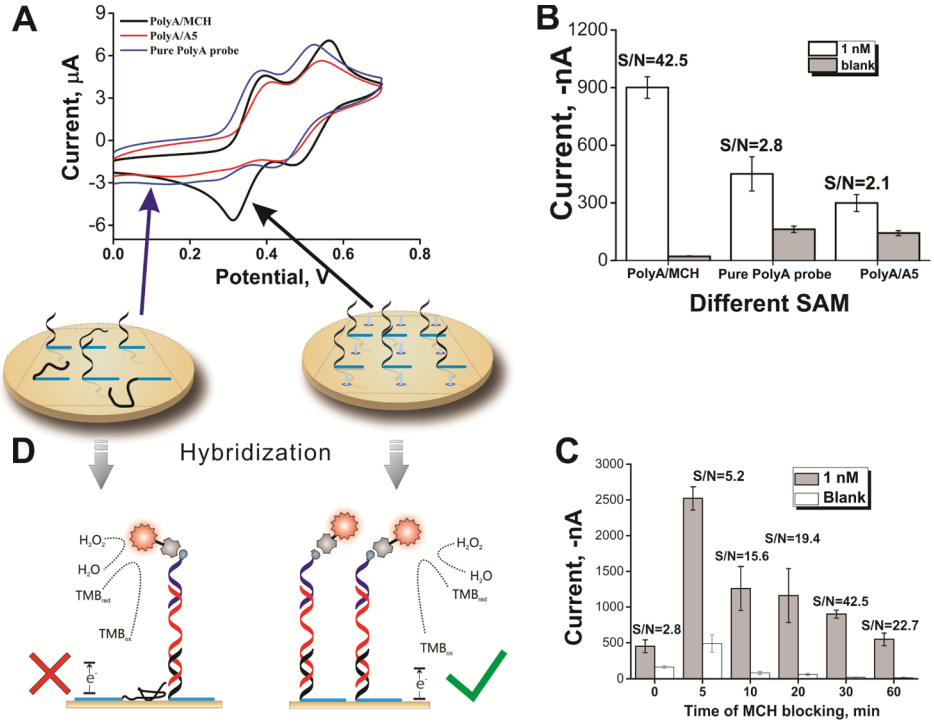

Figure 3. (A) CV curves of TMB on electrode covered with: pure polyA-P (blue curve), polyA-P together with A5 (red curve), and polyA-P together with MCH (black curve); (B) *I*–*t* analysis results of 1 nM target DNA based on different SAMs. Error bars represent standard deviation (SD) of three repetitive experiments; (C) analysis results of 1 nM target DNA using different MCH deposition time; and (D) schematic illustration of the MCH co-assembling.

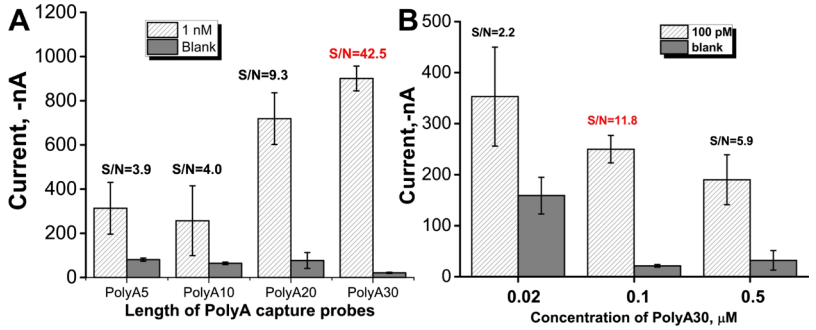

Figure 4. (A) Analysis results of 1 nM target DNA and blank using polyA-P with different lengths of polyA block (5, 10, 20, and 30 nt, respectively). (B) Analysis results of target DNA (100 pM) and blank using varied concentrations of polyA30-tailed capture probes. Error bars are SD of three repetitive experiments using three different electrodes.

3.3.4. Optimization of MCH Deposition Time. Next, the MCH deposition time was further studied to achieve an optimized molecular ratio between the DNA probe and MCH on the electrode surface. In this part, the analysis effect was evaluated by analyzing 1 nM target under different MCH modification time while all other experiment conditions were fixed. As shown in Figure 3C, when MCH was added to the surface with increased reaction time from 10 to 60 min, the background decreased dramatically because MCH replaced most of the unspecific adsorption of DNA and enzyme, and meanwhile, the signal slightly decreased after 10 min maybe because some polyA-Ps were replaced by MCH molecules. Finally, we obtained the highest S/N when the MCH reaction time was 30 min, which was then adopted as the optimized experiment condition during all the following research.

3.3.5. I–t Analysis Performance of Different SAMs. Finally, when 1 nM target DNA was analyzed by utilizing *I*–*t* analysis with three different SAM (polyA-P/MCH, pure polyA-P, and polyA-P/A5), a significantly better S/N was achieved with the polyA-P/MCH sensor, which was at least 15-folds higher than that from the other two SAMs (Figure 3B). This result suggested the better electrochemical performance of the MCH-modified SAM.

3.4. Optimization of PolyA-P Assembling. *3.4.1. Length of the PolyA Tail.* The surface density of the capture probe on the electrode is recognized as an important factor for the DNA hybridization efficiency; thus, in this work, the density of polyA-P was systematically studied by varying the length of the polyA block in the capture probes, toward an optimized performance of our biosensor.

The assembling density of polyA-P on the gold electrode was determined using a reported method.[48] Exactly as expected, the surface density decreased from 2.1 to 0.4 pmol/cm^2, when the length of the polyA block in the capture probe was increased

DOI: 10.1021/acsami.7b17327
ACS Appl. Mater. Interfaces 2018, 10, 6895–6903

from 5 bases to 40 bases (Figure S2) because more surface area was occupied by the polyA blocks of the capture probes on the electrode.

When a sample of 1 nM target DNA was utilized to investigate the analysis performance of the biosensor with the polyA length gradually increasing from polyA5 to polyA30, the current signal increased accordingly, which is a result of the better hybridization efficiency due to lower surface density. On the other hand, the background signal roughly decreased when the length of the polyA tail increased (Figure 4A), and finally, the highest S/N value was achieved with polyA30.

3.4.2. Concentration of PolyA30 Capture Probe (PolyA30-P). Then, we studied the concentration of polyA30-P which affected the final amount of capture probes on the electrode. As shown in Figure 4B, when the concentration of polyA30-P was increased, with an inevitable result of increased surface density, the electrochemical signal decreased accordingly, which was highly consistent with the study above. Finally, the highest S/N value was achieved with 0.1 μM polyA30-P; thus, in the following experiments, 0.1 μM polyA30-P was employed as an optimized condition.

3.5. Detection Performance of PolyA-Based DNA Sensors. *3.5.1. Sensitivity of the PolyA-Based DNA Sensor.* Under the optimum conditions described above, we investigated the sensitivity of our biosensor in the presence of different concentrations of target DNA. As shown in Figures 5 and S3, the electrochemical current signal obviously increased with the increase of the target DNA concentration ranging from 10 fM to 1000 pM (six orders of magnitude). The inset histogram in Figure 5 shows the signal gain for low-concentration targets: the electrochemical current signal has a good linear relationship with the logarithm of target DNA concentration from 0.01 to 1 pM, with a linear correlation coefficient (R^2) of 0.988: $y = 26.4 \lg x + 109.6$, where x is the concentration of DNA and y is the electrochemical current signal. The LOD was thus calculated to be 5 fM, when $x = S_0 + 3\delta$ (S_0 = 31.73 nA is the background signal and δ = 5.56 nA is the SD of S_0).

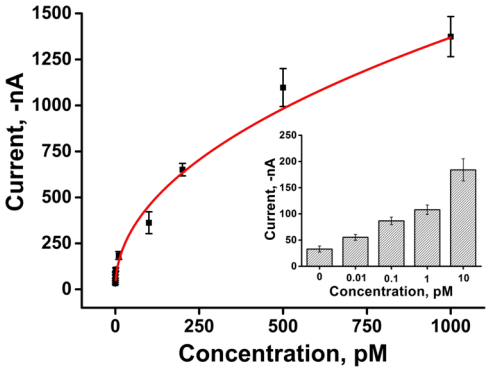

Figure 5. Detection results of target DNA using our DNA sensor. The inserted histogram is the analysis result of low-concentration DNA, and a buffer solution was analyzed for the blank signal. Error bars are the SD across three repetitive experiments using three different electrodes.

3.5.2. Regeneration and Stability of the PolyA-Based DNA Sensor. Regenerability and stability are considered as important indicators for the practicability of a biosensor. To test the regeneration of our biosensor, an electrode, which has been used once for the analysis, was treated with urea solution (8 M) to break the DNA duplexes on the electrode surface and then applied again for the analysis of 1 nM target DNA sample, and the whole process was repeated and recorded several times. As shown in Figure 6, we compared the results from each regeneration step, and two main results are worth noting: (1) equivalent level of current signal could be recovered for at least four times after every "urea-cleaning" and "re-hybridization" operation, which strongly proved the fact that the conformation and amount of the capture probes on the electrode surface was perfectly maintained during the regeneration process. (2) The background signal decreased to lower than 15 nA, which was even better than the blank signal before hybridization, indicating that the DNA duplex and HRP enzyme were adequately removed by conveniently incubating in urea solution.

For stability investigation, the polyA30-P/MCH-modified electrode was stored in TE buffer under 4 °C for 7 days and then applied it for the analysis of 1 nM target. The current signal was found to be impressively stable with only slight signal attenuation (less than 10%), and the SD of the group of electrodes after 7-day storage was only 120 nA (Figure 6B). Benefitting from the strong combination between polyA and the gold electrode and the optimized interface status of the SAM, we successfully achieved excellent stability and reproducibility of our biosensor, which is important for the reliability and economic cost.

3.5.3. Analysis of the PCR Product from Bacterial DNA. Finally, we investigated the practicability of our biosensor by

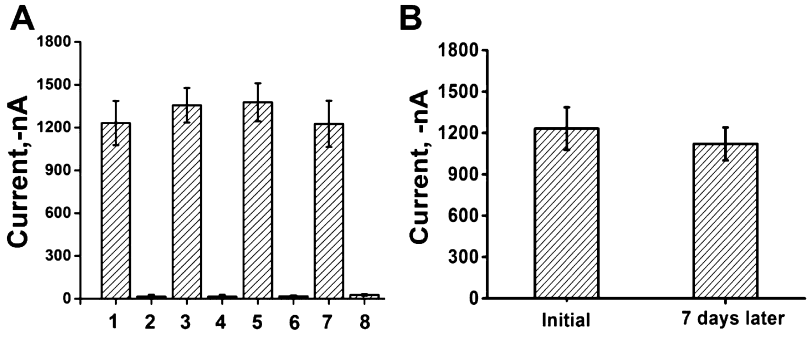

Figure 6. (A) Regenerability test results of the polyA-based DNA sensor with 1 nM target DNA: (1) first-round detection, (2) first-round regeneration, (3) second-round detection, (4) second-round regeneration, (5) third-round detection, (6) third-round regeneration, (7) fourth-round detection, and (8) fourth-round regeneration. (B) Stability test results of the polyA-based electrochemical DNA sensor with 1 nM target DNA: the left column was the initial result and the right column was the result from an electrode, which has been stored for 7 days at 4 °C.

DOI: 10.1021/acsami.7b17327
ACS Appl. Mater. Interfaces 2018, 10, 6895−6903

detecting the PCR product, and the *E. coli* DH5α genomic DNA was used as the template. In this work, asymmetric PCR was employed to produce a 250 nt single-strand DNA (ssDNA) following a reported protocol.[49] As shown in Figure 7, when

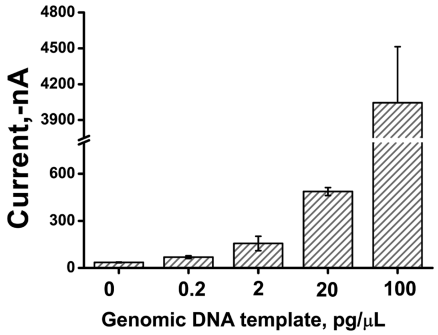

Figure 7. Analysis result of the PCR product from *E. coli* genomic DNA by using the polyA-based DNA sensor.

PCR amplicons from different levels of genomic DNA template was analyzed by our biosensor, the current signal increased along with the increase of the template concentration, and as few as 0.2 pg/μL DNA template in 100 μL unpurified PCR product was successfully detected, which was at least 4 orders of magnitude lower than the conventional electrophoresis (Figure S4). The results strongly demonstrated the promising potential in the fast analysis for pathogenic microorganism DNA.

4. CONCLUSIONS

In summary, we constructed a novel electrochemical biosensor interface, based on the high adenine−gold adsorption affinity, which was successfully applied for the development of a simple, economical, and sensitive electrochemical DNA biosensor. In a considerable number of reported studies, the polyA-based assembling process has been adopted on different analysis platforms, including X-ray photoelectron spectroscopy (XPS), colorimetric,[50] fluorescence,[51] electrochemiluminescent (ECL),[52] and Raman methods,[53] but when applied for the electrochemical DNA analysis, several critical issues were found. First, different co-assembling molecules were systematically studied among polyA-P, A5, and MCH, toward an optimized electron-transfer effect, through comparison of the CV curves, electron-transfer rate, and finally S/N ratio, the obvious superiority of the polyA-P/MCH SAM was strongly demonstrated; second, by varying the numbers of polyA in the capture probe, we modulated the surface density on electrode and successfully improved the hybridization efficiency.

Importantly, several critical experiment conditions were optimized, including the reaction time of MCH and the concentration of the capture probe. Finally, excellent biosensor performance was obtained for the polyA-based electrochemical biosensor. Our polyA-based electrochemical biosensor successfully achieved an LOD as low as 5 fM, which is quite competitive in electrochemical DNA biosensors using similar "sandwich-type" strategies (Table 2), and excellent practicability was demonstrated by analyzing a PCR product from *E. coli* genome with the template level of 0.2 pg/μL, and we believe the analysis capability could be further improved by introducing signal amplification strategies including nanomaterials and RCA probes. On the basis of the ideal electrochemical interface, our polyA-based biosensor exhibited excellent reproducibility and stability, which we believe endow the strategy with great potential for onsite analysis.

■ ASSOCIATED CONTENT

Supporting Information

The Supporting Information is available free of charge on the ACS Publications website at DOI: 10.1021/acsami.7b17327.

Cyclic voltammograms and the linear relationship of peak current versus scan rate; chronocoulometric curves for the gold electrodes; amperometric curves of a series of synthetic target DNA; and electrophoretic analysis results of the asymmetric PCR amplicons (PDF)

■ AUTHOR INFORMATION

Corresponding Authors

*E-mail: lijiang@sinap.ac.cn. Phone: +86 21 39194611 (J.L.).
*E-mail: wenyl@simt.com.cn. Phone: +86 21 38839800 (Y.W.).
*E-mail: liug@simt.com.cn. Phone: +86 21 38839800 (G.L.).

ORCID

Ali Aldalbahi: 0000-0003-1644-2367
Lihua Wang: 0000-0002-6198-7561
Jiang Li: 0000-0003-2372-6624
Gang Liu: 0000-0003-3779-7212

Notes

The authors declare no competing financial interest.

■ ACKNOWLEDGMENTS

This work was financially supported by the National Quality Infrastructure Program of China (2017YFF0204605), National Natural Science Foundation of China (nos. 21775104, 21775102, 21675167, 21505148, U1532119), Shanghai Rising-Star Program (16QB1403100), The Natural Science Foundation of Shanghai 17ZR1412100 15ZR1448400, Na-

Table 2. Comparison of Similar DNA Biosensors Based on "Sandwich-Type" Strategies

number	probes	detection platform	dynamic range	LOD
1	amino-modified probe[54]	electrochemi-luminescence (ECL)	2−16 nM	0.6 nM
2	SH-DNA probe on gold nanorod[55]	UV−vis spectra	0.25−20 nM	
3	SH-DNA probe on gold electrode[32]	electrochemistry	1 pM to 10 nM	1 pM
4	SH-DNA probe on gold nanoparticle-modified graphene oxide[56]	electrochemistry	0.37−10 nM	160 pM
5	DNA nanostructural probe[57]	electrochemistry	10 fM to 10 nM	
6	amino-modified probe on silver-deposited gold nanoparticles[58]	electrochemistry	1.0−70 pM	0.3 pM
7	SH DNA probe on gold nanoparticles[59]	electrochemistry	1 pM to 100 nM	1 pM
8	SH DNA probe on HRP-functionalized Fe_3O_4 nanoparticles[60]	electrochemistry	50 pM to 500 nM	7.1 pM
9	label-free DNA probe on gold electrode (our work)	electrochemistry	10 fM to 10 nM	5 fM

DOI: 10.1021/acsami.7b17327
ACS Appl. Mater. Interfaces 2018, 10, 6895−6903

tional Key R&D Program of China (2016YFA0400900), and the Key Research Program of Frontier Sciences, CAS, grant no. QYZDJ-SSW-SLH031. A.A. would like to extend his sincere appreciation to the Deanship of Scientific Research at King Saud University for funding this work (RG-1436-005).

REFERENCES

(1) Zeng, D.; Wang, Z.; Meng, Z.; Wang, P.; San, L.; Wang, W.; Aldalbahi, A.; Li, L.; Shen, J.; Mi, X. DNA Tetrahedral Nanostructure-Based Electrochemical miRNA Biosensor for Simultaneous Detection of Multiple miRNAs in Pancreatic Carcinoma. *ACS Appl. Mater. Interfaces* **2017**, *9*, 24118−24125.

(2) Yang, C.; Shi, K.; Dou, B.; Xiang, Y.; Chai, Y.; Yuan, R. In Situ DNA-Templated Synthesis of Silver Nanoclusters for Ultrasensitive and Label-Free Electrochemical Detection of MicroRNA. *ACS Appl. Mater. Interfaces* **2015**, *7*, 1188−1193.

(3) Dong, S.; Zhao, R.; Zhu, J.; Lu, X.; Li, Y.; Qiu, S.; Jia, L.; Jiao, X.; Song, S.; Fan, C.; Hao, R.; Song, H. Electrochemical DNA Biosensor Based on a Tetrahedral Nanostructure Probe for the Detection of Avian Influenza A (H7N9) Virus. *ACS Appl. Mater. Interfaces* **2015**, *7*, 8834−8842.

(4) Hou, T.; Li, W.; Liu, X.; Li, F. Label-Free and Enzyme-Free Homogeneous Electrochemical Biosensing Strategy Based on Hybridization Chain Reaction: A Facile, Sensitive, and Highly Specific MicroRNA Assay. *Anal. Chem.* **2015**, *87*, 11368−11374.

(5) Gai, P.; Gu, C.; Li, H.; Sun, X.; Li, F. Ultrasensitive Ratiometric Homogeneous Electrochemical MicroRNA Biosensing via Target-Triggered Ru(III) Release and Redox Recycling. *Anal. Chem.* **2017**, *89*, 12293−12298.

(6) Pei, H.; Liang, L.; Yao, G.; Li, J.; Huang, Q.; Fan, C. Reconfigurable Three-Dimensional DNA Nanostructures for the Construction of Intracellular Logic Sensors. *Angew. Chem., Int. Ed.* **2012**, *51*, 9020−9024.

(7) Lapierre, M. A.; O'Keefe, M.; Taft, B. J.; Kelley, S. O. Electrocatalytic Detection of Pathogenic DNA Sequences and Antibiotic Resistance Markers. *Anal. Chem.* **2003**, *75*, 6327−6333.

(8) Yang, F.; Zuo, X.; Li, Z.; Deng, W.; Shi, J.; Zhang, G.; Huang, Q.; Song, S.; Fan, C. A Bubble-Mediated Intelligent Microscale Electrochemical Device for Single-Step Quantitative Bioassays. *Adv. Mater.* **2014**, *26*, 4671−4676.

(9) Ge, Z.; Pei, H.; Wang, L.; Song, S.; Fan, C. Electrochemical Single Nucleotide Polymorphisms Genotyping on Surface Immobilized Three-Dimensional Branched DNA Nanostructure. *Sci. China: Chem.* **2011**, *54*, 1273−1276.

(10) Wan, Y.; Wang, P.; Su, Y.; Wang, L.; Pan, D.; Aldalbahi, A.; Yang, S.; Zuo, X. Nanoprobe-Initiated Enzymatic Polymerization for Highly Sensitive Electrochemical DNA Detection. *ACS Appl. Mater. Interfaces* **2015**, *7*, 25618−25623.

(11) Yao, G.; Pei, H.; Li, J.; Zhao, Y.; Zhu, D.; Zhang, Y.; Lin, Y.; Huang, Q.; Fan, C. Clicking DNA to Gold Nanoparticles: Poly-Adenine-Mediated Formation of Monovalent DNA-Gold Nanoparticle Conjugates with Nearly Quantitative Yield. *NPG Asia Mater.* **2015**, *7*, No. e159.

(12) Lapierre-Devlin, M. A.; Asher, C. L.; Taft, B. J.; Gasparac, R.; Roberts, M. A.; Kelley, S. O. Amplified Electrocatalysis at DNA-Modified Nanowires. *Nano Lett.* **2005**, *5*, 1051−1055.

(13) Kelley, S. O.; Boon, E. M.; Barton, J. K.; Jackson, N. M.; Hill, M. G. Single-Base Mismatch Detection Based on Charge Transduction Through DNA. *Nucleic Acids Res.* **1999**, *27*, 4830−4837.

(14) Fan, C.; Plaxco, K. W.; Heeger, A. J. Electrochemical Interrogation of Conformational Changes as A Reagentless Method for the Sequence-Specific Detection of DNA. *Proc. Natl. Acad. Sci. U.S.A.* **2003**, *100*, 9134−9137.

(15) Lin, M.; Wen, Y.; Li, L.; Pei, H.; Liu, G.; Song, H.; Zuo, X.; Fan, C.; Huang, Q. Target-Responsive, DNA Nanostructure-Based E-DNA Sensor for MicroRNA Analysis. *Anal. Chem.* **2014**, *86*, 2285−2288.

(16) Liu, G.; Lao, R.; Xu, L.; Xu, Q.; Li, L.; Zhang, M.; Shen, H.; Mathur, S.; Fan, C.; Song, S. Detection of Single-Nucleotide Polymorphism on uidA Gene of Escherichia coli by a Multiplexed Electrochemical DNA Biosensor with Oligonucleotide-Incorporated Nonfouling Surface. *Sensors* **2011**, *11*, 8018−8027.

(17) Liu, G.; Lao, R.; Xu, L.; Xu, Q.; Li, L.; Zhang, M.; Song, S.; Fan, C. Single-nucleotide Polymorphism Genotyping Using a Novel Multiplexed Electrochemical Biosensor with Nonfouling Surface. *Biosens. Bioelectron.* **2013**, *42*, 516−521.

(18) Ricci, F.; Lai, R. Y.; Heeger, A. J.; Plaxco, K. W.; Sumner, J. J. Effect of Molecular Crowding on the Response of An Electrochemical DNA Sensor. *Langmuir* **2007**, *23*, 6827−6834.

(19) Su, S.; Cao, W.; Liu, W.; Lu, Z.; Zhu, D.; Chao, J.; Weng, L.; Wang, L.; Fan, C.; Wang, L. Dual-Mode Electrochemical Analysis of MicroRNA-21 Using Gold Nanoparticle-Decorated MoS2 Nanosheet. *Biosens. Bioelectron.* **2017**, *94*, 552−559.

(20) Su, S.; Sun, H.; Cao, W.; Chao, J.; Peng, H.; Zuo, X.; Yuwen, L.; Fan, C.; Wang, L. Dual-Target Electrochemical Biosensing Based on DNA Structural Switching on Gold Nanoparticle-Decorated MoS2 Nanosheets. *ACS Appl. Mater. Interfaces* **2016**, *8*, 6826−6833.

(21) Wen, Y.; Liu, G.; Pei, H.; Li, L.; Xu, Q.; Liang, W.; Li, Y.; Xu, L.; Ren, S.; Fan, C. DNA Nanostructure-based Ultrasensitive Electrochemical microRNA Biosensor. *Methods* **2013**, *64*, 276−282.

(22) Wen, Y.; Pei, H.; Wan, Y.; Su, Y.; Huang, Q.; Song, S.; Fan, C. DNA Nanostructure-Decorated Surfaces for Enhanced Aptamer-Target Binding and Electrochemical Cocaine Sensors. *Anal. Chem.* **2011**, *83*, 7418−7423.

(23) Wen, Y.; Wang, L.; Xu, L.; Li, L.; Ren, S.; Cao, C.; Jia, N.; Aldalbahi, A.; Song, S.; Shi, J.; Xia, J.; Liu, G.; Zuo, X. Electrochemical Detection of PCR Amplicons of Escherichia Coli Genome Based on DNA Nanostructural Probes and PolyHRP Enzyme. *Analyst* **2016**, *141*, 5304−5310.

(24) Shi, X.-M.; Fan, G.-C.; Shen, Q.; Zhu, J.-J. Photoelectrochemical DNA Biosensor Based on Dual-Signal Amplification Strategy Integrating Inorganic-Organic Nanocomposites Sensitization with λ-Exonuclease-Assisted Target Recycling. *ACS Appl. Mater. Interfaces* **2016**, *8*, 35091−35098.

(25) Kou, B.-B.; Zhang, L.; Xie, H.; Wang, D.; Yuan, Y.-L.; Chai, Y.-Q.; Yuan, R. DNA Enzyme-Decorated DNA Nanoladders as Enhancer for Peptide Cleavage-Based Electrochemical Biosensor. *ACS Appl. Mater. Interfaces* **2016**, *8*, 22869−22874.

(26) Zhang, J.; Song, S.; Wang, L.; Pan, D.; Fan, C. A Gold Nanoparticle-based Chronocoulometric DNA Sensor for Amplified Detection of DNA. *Nat. Protoc.* **2007**, *2*, 2888−2895.

(27) Choi, J.-H.; Kim, H.; Choi, J.-H.; Choi, J.-W.; Oh, B.-K. Signal Enhancement of Silicon Nanowire-Based Biosensor for Detection of Matrix Metalloproteinase-2 Using DNA-Au Nanoparticle Complexes. *ACS Appl. Mater. Interfaces* **2013**, *5*, 12023−12028.

(28) Chen, P.; Pan, D.; Fan, C.; Chen, J.; Huang, K.; Wang, D.; Zhang, H.; Li, Y.; Feng, G.; Liang, P.; He, L.; Shi, Y. Gold Nanoparticles for High-Throughput Genotyping of Long-Range Haplotypes. *Nat. Nanotechnol.* **2011**, *6*, 639−644.

(29) Gui, A. L.; Luais, E.; Peterson, J. R.; Gooding, J. J. Zwitterionic Phenyl layers: Finally, Stable, Anti-Biofouling Coatings That Do Not Passivate Electrodes. *ACS Appl. Mater. Interfaces* **2013**, *5*, 4827−4835.

(30) Liu, G.; Wan, Y.; Gau, V.; Zhang, J.; Wang, L.; Song, S.; Fan, C. An Enzyme-Based E-DNA Sensor for Sequence-Specific Detection of Femtomolar DNA Targets. *J. Am. Chem. Soc.* **2008**, *130*, 6820−6825.

(31) Das, J.; Ivanov, I.; Sargent, E. H.; Kelley, S. O. DNA Clutch Probes for Circulating Tumor DNA Analysis. *J. Am. Chem. Soc.* **2016**, *138*, 11009−11016.

(32) Zhang, J.; Lao, R.; Song, S.; Yan, Z.; Fan, C. Design of An Oligonucleotide-Incorporated Nonfouling Surface and Its Application in Electrochemical DNA Sensors for Highly Sensitive and Sequence-Specific Detection of Target DNA. *Anal. Chem.* **2008**, *80*, 9029−9033.

(33) Zhang, J.; Wang, L.; Pan, D.; Song, S.; Fan, C. DNA Hybridization "turns on" Electrocatalysis at Gold Electrodes. *Chem. Commun.* **2007**, 1154−1156.

(34) Herne, T. M.; Tarlov, M. J. Characterization of DNA Probes Immobilized on Gold Surfaces. *J. Am. Chem. Soc.* **1997**, *119*, 8916−8920.

DOI: 10.1021/acsami.7b17327
ACS Appl. Mater. Interfaces 2018, 10, 6895−6903

(35) Lao, R.; Song, S.; Wu, H.; Wang, L.; Zhang, Z.; He, L.; Fan, C. Electrochemical Interrogation of DNA Monolayers on Gold Surfaces. *Anal. Chem.* **2005**, *77*, 6475−6480.
(36) Schreiner, S. M.; Shudy, D. F.; Hatch, A. L.; Opdahl, A.; Whitman, L. J.; Petrovykh, D. Y. Controlled and Efficient Hybridization Achieved with DNA Probes Immobilized Solely through Preferential DNA-Substrate Interactions. *Anal. Chem.* **2010**, *82*, 2803−2810.
(37) Opdahl, A.; Petrovykh, D. Y.; Kimura-Suda, H.; Tarlov, M. J.; Whitman, L. J. Independent Control of Grafting Density and Conformation of Single-Stranded DNA Brushes. *Proc. Natl. Acad. Sci. U.S.A.* **2007**, *104*, 9−14.
(38) Koo, K. M.; Sina, A. A. I.; Carrascosa, L. G.; Shiddiky, M. J. A.; Trau, M. DNA-Bare Gold Affinity Interactions: Mechanism and Applications in Biosensing. *Anal. Methods* **2015**, *7*, 7042−7054.
(39) Koo, K. M.; Sina, A. A. I.; Carrascosa, L. G.; Shiddiky, M. J. A.; Trau, M. DNA-bare Gold Affinity Interactions: Mechanism and Applications in Biosensing. *Anal. Methods* **2015**, *7*, 7042−7054.
(40) Liu, P.; Wang, D.; Zhou, Y.; Wang, H.; Yin, H.; Ai, S. DNA Methyltransferase Detection based on Digestion Triggering the Combination of Poly Adenine DNA with Gold Nanoparticles. *Biosens. Bioelectron.* **2016**, *80*, 74−78.
(41) Kimura-Suda, H.; Petrovykh, D. Y.; Tarlov, M. J.; Whitman, L. J. Base-dependent Competitive Adsorption of Single-stranded DNA on Gold. *J. Am. Chem. Soc.* **2003**, *125*, 9014−9015.
(42) Pei, H.; Li, F.; Wan, Y.; Wei, M.; Liu, H.; Su, Y.; Chen, N.; Huang, Q.; Fan, C. Designed Diblock Oligonucleotide for the Synthesis of Spatially Isolated and Highly Hybridizable Functionalization of DNA-Gold Nanoparticle Nanoconjugates. *J. Am. Chem. Soc.* **2012**, *134*, 11876−11879.
(43) Wu, C.; Zhou, C.; Wang, E.; Dong, S. A Label-free and Enzyme-free System for Operating Various Logic Devices Using Poly(thymine)-templated CuNPs and SYBR Green I as Signal Transducers. *Nanoscale* **2016**, *8*, 14243−14249.
(44) Wang, C.; Zhang, H.; Zeng, D.; Sun, W.; Zhang, H.; Aldalbahi, A.; Wang, Y.; San, L.; Fan, C.; Zuo, X.; Mi, X. Elaborately Designed Diblock Nanoprobes for Simultaneous Multicolor Detection of MicroRNAs. *Nanoscale* **2015**, *7*, 15822−15829.
(45) Yang, X.; Li, J.; Pei, H.; Zhao, Y.; Zuo, X.; Fan, C.; Huang, Q. DNA-gold Nanoparticle Conjugates-based Nanoplasmonic Probe for Specific Differentiation of Cell Types. *Anal. Chem.* **2014**, *86*, 3227−3231.
(46) Chen, N.; Wei, M.; Sun, Y.; Li, F.; Pei, H.; Li, X.; Su, S.; He, Y.; Wang, L.; Shi, J.; Fan, C.; Huang, Q. Self-assembly of Poly-adenine-tailed CpG Oligonucleotide-gold Nanoparticle Nanoconjugates with Immunostimulatory Activity. *Small* **2014**, *10*, 368−375.
(47) Laviron, E. General Expression of the Linear Potential Sweep Voltammogram in the Case of Diffusionless Electrochemical Systems. *J. Electroanal. Chem.* **1979**, *101*, 19−28.
(48) Steel, A. B.; Herne, T. M.; Tarlov, M. J. Electrochemical Quantitation of DNA Immobilized on Gold. *Anal. Chem.* **1998**, *70*, 4670−4677.
(49) Lai, R. Y.; Lagally, E. T.; Lee, S.-H.; Soh, H. T.; Plaxco, K. W.; Heeger, A. J. Rapid, Sequence-specific Detection of Unpurified PCR Amplicons via a Reusable, Electrochemical Sensor. *Proc. Natl. Acad. Sci. U.S.A.* **2006**, *103*, 4017−4021.
(50) Chen, L.; Chao, J.; Qu, X.; Zhang, H.; Zhu, D.; Su, S.; Aldalbahi, A.; Wang, L.; Pei, H. Probing Cellular Molecules with PolyA-Based Engineered Aptamer Nanobeacon. *ACS Appl. Mater. Interfaces* **2017**, *9*, 8014−8020.
(51) Zhou, C. Y.; Wu, C. T.; Liu, Y. Q.; Wang, E. K. Effective Construction of a AuNPs-DNA System for the Implementation of Various Advanced Logic Gates. *RSC Adv.* **2016**, *6*, 106641−106647.
(52) Guillou, F.; Porcari, G.; Yibole, H.; van Dijk, N.; Brück, E. Taming the first-order transition in giant magnetocaloric materials. *Adv. Mater.* **2014**, *26*, 2671−2675.
(53) Hu, C. Y.; Shen, J. L.; Yan, J.; Zhong, J.; Qin, W. W.; Liu, R.; Aldalbahi, A.; Zuo, X. L.; Song, S. P.; Fan, C. H.; He, D. N. Highly Narrow Nanogap-containing Au@Au Core-shell SERS Nanoparticles: Size-dependent Raman Enhancement and Applications in Cancer Cell Imaging. *Nanoscale* **2016**, *8*, 2090−2096.
(54) Spehar-Délèze, A.-M.; Gransee, R.; Martinez-Montequin, S.; Bejarano-Nosas, D.; Dulay, S.; Julich, S.; Tomaso, H.; O'Sullivan, C. K. Electrochemiluminescence DNA Sensor Array for Multiplex Detection of Biowarfare Agents. *Anal. Bioanal. Chem.* **2015**, *407*, 6657−6667.
(55) Parab, H. J.; Jung, C.; Lee, J.-H.; Park, H. G. A Gold Nanorod-based Optical DNA Biosensor for the Diagnosis of Pathogens. *Biosens. Bioelectron.* **2010**, *26*, 667−673.
(56) Saeed, A. A.; Sánchez, J. L. A.; O'Sullivan, C. K.; Abbas, M. N. DNA Biosensors Based on Gold Nanoparticles-modified Graphene Oxide for the Detection of Breast Cancer Biomarkers for Early Diagnosis. *Bioelectrochemistry* **2017**, *118*, 91−99.
(57) Wen, Y.; Wang, L.; Xu, L.; Li, L.; Ren, S.; Cao, C.; Jia, N.; Aldalbahi, A.; Song, S.; Shi, J.; Xia, J.; Liu, G.; Zuo, X. Electrochemical Detection of PCR Amplicons of Escherichia Coli Genome Based on DNA Nanostructural Probes and PolyHRP Enzyme. *Analyst* **2016**, *141*, 5304−5310.
(58) Zhang, Y.; Geng, X.; Ai, J.; Gao, Q.; Qi, H.; Zhang, C. Signal Amplification Detection of DNA using a Sensor Fabricated by One-step Covalent Immobilization of Amino-terminated Probe DNA onto the Polydopamine-modified Screen-printed Carbon Electrode. *Sens. Actuators, B* **2015**, *221*, 1535−1541.
(59) Liu, J.; Tian, M.; Liang, Z. DNA Analysis Based on the Electrocatalytic Amplification of Gold Nanoparticles. *Electrochim. Acta* **2013**, *113*, 186−193.
(60) Dong, X.-Y.; Mi, X.-N.; Wang, B.; Xu, J.-J.; Chen, H.-Y. Signal Amplification for DNA Detection Based on the HRP-functionalized Fe3O4 Nanoparticles. *Talanta* **2011**, *84*, 531−537.

DOI: 10.1021/acsami.7b17327
ACS Appl. Mater. Interfaces 2018, 10, 6895−6903